Available online at www.sciencedirect.com

ScienceDirect

Acta Materialia 67 (2014) 134–144

Acta MATERIALIA

www.elsevier.com/locate/actamat

A phase-field model for grain growth with trijunction drag

A.E. Johnson [a], P.W. Voorhees [a,b,*]

[a] Department of Materials Science and Engineering, Northwestern University, Evanston, IL 60208-3108, USA
[b] Department of Engineering Sciences and Applied Mathematics, Northwestern University, Evanston, IL 60208-3108, USA

Received 19 September 2013; received in revised form 5 December 2013; accepted 7 December 2013
Available online 25 January 2014

Abstract

A phase-field model has been developed to study the effect of triple junction (TJ) mobility on 2-D grain growth kinetics. The method captures the results of past work such as a linear increase in the average grain size with time, but can also follow the transition from TJ-limited to grain boundary energy-limited growth. The distribution of grain boundary curvature is examined. In the low TJ mobility simulations the distribution has a peak at zero curvature and approaches the grain boundary mobility-limited steady-state distribution at larger sizes. Even for extremely low TJ mobility, a small fraction of the grain boundary length has non-zero curvature and thus a lack of self-similarity is observed for all TJ-limited simulations, even when the average size is increasing linearly in time. We find that the topology of the grain structure is independent of the degree of TJ drag, within the range of parameters employed in the simulation. The effects of TJ mobility increase as the grain size decreases, suggesting that TJ mobility can play a significant role in nanocrystalline grain growth kinetics.

Keywords: Grain growth; Triple junction drag; Computer simulation

1. Introduction

Grain growth and coarsening occur in many polycrystalline materials in order to reduce the interfacial free energy of the system. Especially during high-temperature processing and operation, the grain growth rate can be significant and can greatly affect properties such as yield strength.

Triple junctions (TJs), the line formed by the intersection of three grains, play an important role in grain growth kinetics due to their energy [1], mobility [2], impurity affinity [3] and larger volume fraction for small-grained materials [4]. TJs can thus also significantly affect properties, e.g. creep via enhanced diffusivity [5–7] or electrochemical corrosivity via enhanced electron mobility along triple lines [8]. In small-grained materials, there may be many competing mechanisms and driving forces that affect grain growth. However, it has been shown theoretically that TJs are more effective at "dragging" the growth rate of nanocrystalline grains, relative to vacancies, particles and impurities [9].

TJs are often assumed to have large mobility relative to the grain boundaries and thus move with the grain boundaries in order to maintain the TJ equilibrium angles [10]. However, as grain size decreases and approaches the nanoscale, the influence of TJs relative to grain boundaries increases [11–14]. In particular, TJs can have low mobility in small grains or at low temperatures and can significantly affect grain boundary curvatures, TJ angles and the overall kinetics [15,2,16–23].

As the TJ mobility approaches zero, the grain boundary curvatures approach zero and the driving force for grain growth becomes the deviation of the TJ angles from their equilibrium values. Tricrystal experiments have shown that the TJ angles deviate from equilibrium as the temperature decreases, suggesting that kinetics are grain boundary mobility limited at high temperatures and TJ mobility limited at low temperatures [2,16,20]. This temperature

* Corresponding author at: Department of Materials Science and Engineering, Northwestern University, Evanston, IL 60208-3108, USA.
E-mail address: p-voorhees@northwestern.edu (P.W. Voorhees).

1359-6454/$36.00
http://dx.doi.org/10.1016/j.actamat.2013.12.012

dependence of Zn tricrystals and bicrystals was shown to exhibit Arrhenius behavior, with TJs having a larger activation energy [16]. Furthermore, it has been proposed that low TJ mobility results in linear growth kinetics, i.e. $\langle D\rangle \sim t$ where $\langle D\rangle$ is the average grain size [15,2,16]. Such kinetics have been observed in nanocrystalline Fe [24,25] and molecular dynamics simulations of nanocrystalline Ni [26].

Importantly, TJ mobility has a larger effect for smaller grains, suggesting that nanocrystalline grain growth kinetics is largely determined by TJ mobility. Thus it is essential to understand TJ mobility in order to understand nanocrystalline grain growth kinetics as well as to design and build robust nanocrystalline materials. In particular, accurately modeling TJ mobility is important for predicting the effect of TJs on grain growth and grain stabilization in nanocrystalline materials [27,2]. Molecular dynamics [28,19], network [22], virtual vertex [29,23] and Potts [30] models have been used to model TJ drag, demonstrating results mostly consistent with theory and experiment. The vertex models and Potts models have observed linear kinetics, as well as a widening of the grain size distribution and a lack of self-similarity during TJ mobility-limited grain growth.

The phase-field model, however, has the advantage of smooth interfaces, no need to explicitly track trijunctions, and the ability to incorporate any number of conserved and non-conserved parameters such as impurity concentration [31,32]. Because impurities have been seen to preferentially segregate to triple lines, it is important to study TJs using a model that can incorporate long-range diffusion. Thus, this model is the first step to combining the effects of diffusion- and TJ-limited grain growth.

2. Theory

2.1. Triple junction mobility

An analytical theory for the simplest TJ geometry – seen in – was developed by Gottstein and Shvindlerman to calculate the TJ velocity, mobility and angle [2,18,15]. The shape of the grain boundary $y(x)$ for the $n < 6$ geometry is given by:

$$y(x) = \xi \arccos\left[e^{-\frac{x}{\xi}+c_1}\right] + c_2 \tag{1}$$

where $\xi = \frac{a}{2\theta_a}$, $c_1 = \ln(\sin\theta_a)$, $c_2 = -\xi\left(\frac{\pi}{2} - \theta_a\right)$, and n is the number sides of the grain. There are only two degrees of freedom: if the grain size, a, and the dihedral angle, $2\theta_a$, are known, then the grain boundary (GB) shape can be uniquely determined.

For grains with fewer than six sides, the TJ angles inside the grain are less than their equilibrium values and the grain shrinks (middle grain in Fig. 1(a)). In this system with isotropic grain boundary energies, the TJ velocity is:

$$V_{TJ} = m_{TJ}\sigma(2\cos\theta_a - 1) \tag{2}$$

where V_{TJ} is the TJ velocity, m_{TJ} is the TJ mobility, and σ is the grain boundary energy.

By requiring that the TJ velocity be equal to the grain boundary velocity in the x-direction, the mobility parameter, Λ, can be defined:

$$\Lambda = \frac{m_{TJ}a}{m_{GB}} = \frac{2\theta_a}{2\cos\theta_a - 1} \tag{3}$$

where m_{TJ} and m_{GB} are the TJ and GB mobilities. Λ is dimensionless and for a given system describes the relative importance of TJ and grain boundary mobilities. For large m_{TJ} (grain boundary-limited kinetics), Λ is large and the denominator on the right side of Eq. (3) approaches zero and thus θ_a approaches the equilibrium isotropic value of 60°. For small m_{TJ} (TJ-limited kinetics), Λ approaches zero and θ_a approaches zero, and the TJ velocity is dictated by Eq. (2). Decreasing the grain size, a, decreases Λ as well as the TJ angle, and so TJs play a larger role for small grains. Furthermore, by simply measuring the angle and grain size in such a system, the relative TJ and grain boundary mobilities can be determined. A similar analysis can be done for $n > 6$; see Refs. [2,15,18].

For polycrystalline systems, Λ', described by Eq. (4), is used to measure the overall effect of TJs [33,34]:

$$\Lambda' = \frac{m_{TJ}\langle D\rangle}{2m_{GB}} \tag{4}$$

where $\langle D\rangle$ is the average grain size, or effective grain diameter. In polycrystals, the grain growth kinetics is typically described by:

$$\langle D\rangle \sim kt^n \tag{5}$$

where k is a rate constant, and n is the grain growth exponent. Theoretically, growth limited by grain boundary curvature has a growth exponent of 1/2. In two dimensions, Gottstein and Shvindlerman proposed that grain growth can be described by Eq. (6), which consists of a grain boundary term and a TJ term [35,13].

$$\frac{1}{m_{GB}\sigma}\left(\langle D\rangle^2 - \langle D_o\rangle^2\right) + \frac{1}{m_{TJ}\sigma}\left(\langle D\rangle - \langle D_o\rangle\right) = t \tag{6}$$

For small grains, the linear TJ term dominates and $\langle D\rangle \sim t$; the growth exponent is 1. For large grains, the parabolic grain boundary term dominates and $\langle D\rangle \sim \sqrt{t}$; the growth exponent is 1/2. Thus, for small grains the growth is driven by TJ angles, and for large grains it is driven by GB curvature.

Gottstein and Shvindlermann developed equations for the rate of area change of individual grains, comparable to the Von Neumann–Mullins equation, but with TJ mobility taken into account:

$$\frac{dA}{dt}(n) = \frac{m_{GB}\sigma\pi}{3(1+1/\Lambda)}\left(n\frac{6+\sqrt{3}\Lambda}{2+\sqrt{3}\Lambda} - 6\right), \quad n < 6 \tag{7a}$$

$$\frac{dA}{dt}(n) = \frac{m_{GB}\sigma\pi}{3(1+1/\Lambda)}\left(n\left(1 - \frac{6}{\pi\Lambda B}\right) - 6\right), \quad n > 6 \tag{7b}$$

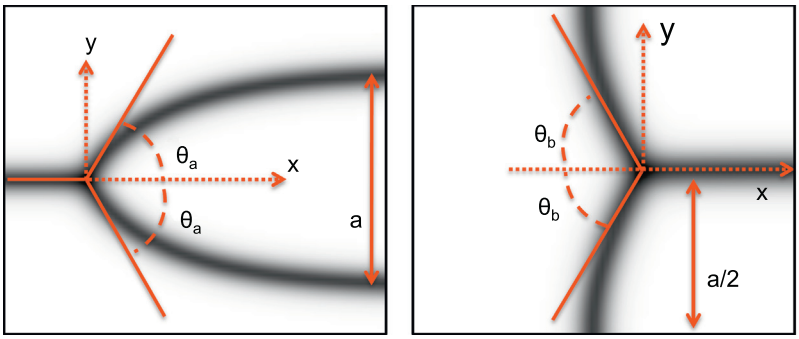

(a) Class $n < 6$ (b) Class $n > 6$

Fig. 1. Steady-state TJ geometries. The TJ moves to the right in both cases. The trijunction angle, θ, and grain boundary shapes have been determined analytically [2,18,15].

where $B = -\frac{\sqrt{3}}{\ln(\sin(\pi/3))}$ and n is the number of sides [17]. These equations were derived by treating the TJs as mobile defects that act to partially pin the grain boundaries. These are considered mixed kinetics, i.e. the TJ angles do not deviate significantly from their equilibrium angles, such that $5 < \Lambda < 25$. In calculating Λ, a is the TJ spacing for the grain class n [34]. Gottstein and Shvindlerman also proposed a pure TJ-limited theory for dA/dt in which the grains are approximated to be regular polyhedra [18]:

$$\frac{dA}{dt}(n) = m_{TJ}\sigma P \cos\left(\frac{\pi}{n}\right)\left(2\sin\left(\frac{\pi}{n}\right) - 1\right) \tag{8}$$

where P is the perimeter for n-sided polyhedra. This equation requires that $\Lambda \ll 1$. It is clear that for $1 < \Lambda < 5$ neither of these two TJ-mobility theories describes the kinetics with completer accuracy.

2.2. Phase-field model

There are numerous computational techniques for modeling grain growth, including Monte Carlo Potts [36], vertex [37,38], front tracking [39], molecular dynamics [40], phase-field [31,32], network [41] and phase-field crystal [42]. In this work, a multi-order parameter phase-field model has been developed that accounts for TJ mobility in two dimensions.

The multi-order parameter phase-field model of grain growth, developed by Fan and Chen [31,32], is based on the diffuse interface theory for non-conserved motion [43,44]. A system is composed of a number of non-conserved order parameters which represent grain orientations. The driving force for microstructural evolution is the minimization of a free energy functional, which is composed of a bulk free energy term f_o and a gradient term that incorporates the interfacial energy:

$$F = f_o(\eta_1, \eta_2, \ldots, \eta_p) + \sum_{i=1}^{p} \frac{\kappa_i}{2}(\nabla\eta_i)^2 \tag{9}$$

where:

$$f_o(\eta_1, \eta_2, \ldots, \eta_p) = \mu\left(\sum_{i=1}^{p}\left(-\frac{\alpha}{2}\eta_i^2 + \frac{\beta}{4}\eta_i^4\right)\right) + \mu\left(\gamma\sum_{i=1}^{p}\sum_{j\neq i}^{p}\eta_i^2\eta_j^2\right) \tag{10}$$

and κ_i is the gradient energy coefficient, $\eta_1, \eta_2, \ldots, \eta_p$ are the order parameters, and μ, α, β and γ are input phenomenological parameters [31]. The bulk free energy functional has degenerate minima at $f_o(1,0,0,\ldots,0)$, $f_o(0,1,0,\ldots,0)$, etc. The parameters μ, α, β and γ affect the minimum, maximum and height of this energy barrier between order parameters and are chosen to maintain symmetry at the grain boundary: $\alpha = 1,\ \beta = 1,\ \gamma = 1.5,\ \kappa = 1$. The results of this work depend weakly on their exact values.

The evolution of the grain boundaries are governed by the Allen–Cahn equation [44] or the time-dependent Ginzburg–Landau equation, which model non-conserved phenomena:

$$\frac{\partial\eta_i(r,t)}{\partial t} = L_i\frac{\delta F}{\delta\eta_i(r,t)}, \quad i = 1,2,\ldots,p \tag{11}$$

where L_i is the mobility and p is the number of grains in the system.

In this 2-D phase-field system, the sum of the order parameters, $\Phi(i,j) = \sum\eta(i,j)$, is equal to 1.0 at a point (i,j) inside grains and at grain boundaries, and approximately equal to 1.08 at TJs (see Fig. 2). Calculating the sum of the order parameters thus allows us to distinguish TJs from grain boundaries and ultimately to manipulate the TJs and their properties without affecting the grain boundaries. To account for TJ mobility, the Allen–Cahn mobility, L, was altered to be a function of the sum of the order parameters. A low TJ mobility was accomplished by making the function, $L(\Phi)$, a negative Gaussian with a minimum at $\Phi_{min} = 1.04$, described by Eq. (12) and illustrated graphically in Fig. 2.

$$L(i,j) = L_{GB} - exp[-\Phi_{width}(\Phi(i,j) - \Phi_{min})^2]^*[L_{GB} - L_{TJ}] \tag{12}$$

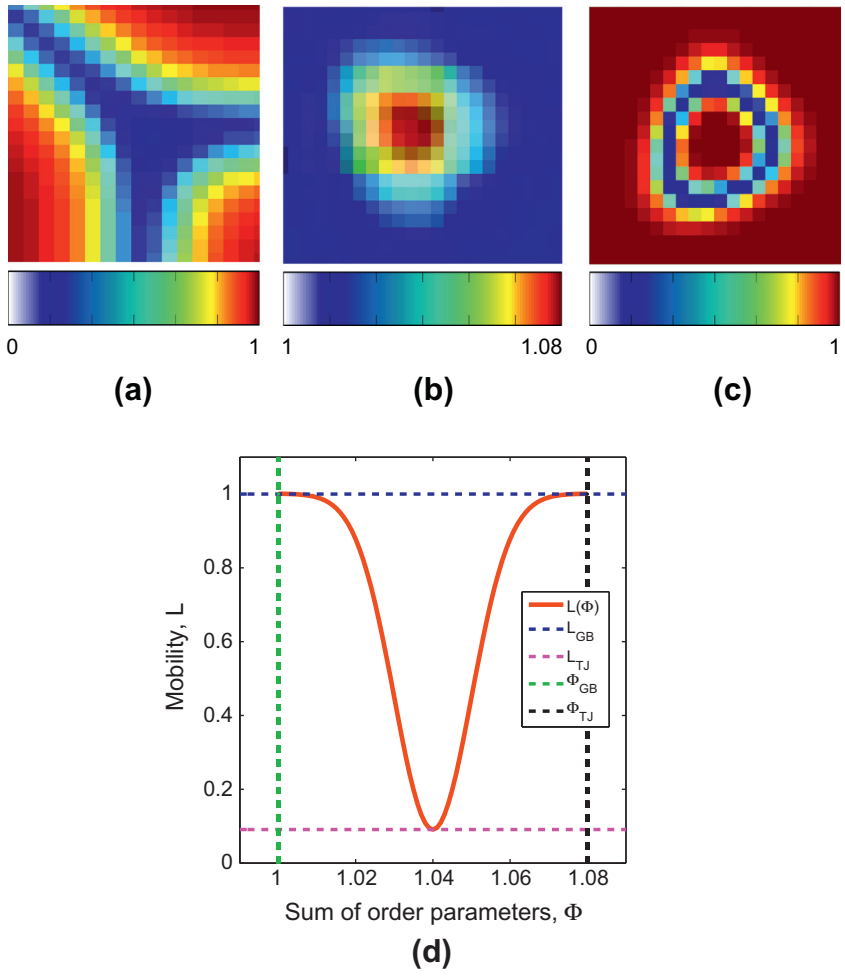

Fig. 2. TJ mobility model. (a) Sum of the order parameters squared at a TJ. (b) Sum of the order parameters at a TJ. (c) Color map of the mobility of the TJ. The center of the TJ is mobile while the area around it is less mobile. (b) Plot of the mobility as a function of the sum of the order parameters. (For interpretation of the references to color in this figure legend, the reader is referred to the web version of this article.)

The grain boundary mobility, L_{GB}, is 1.0. The mobility function was set to be a minimum of L_{TJ} at $\Phi_{min} = 1.04$, halfway between the grain boundary value (1.0) and the TJ value (1.08), in order to maintain the stability of the TJ. Furthermore, Φ_{width} affects the width of the Gaussian in mobility-sum of the order parameter space. Φ_{width} was chosen to be 5000, small enough that grain boundary mobility is not affected and large enough that the ring of low mobility is several mesh points wide.

To measure the effects of TJ mobility, the mean curvature, H, of a diffuse interface can be calculated using:

$$H = \nabla \cdot \frac{\nabla \eta}{|\nabla \eta|} \tag{13}$$

The curvature is determined numerically at each grid point. To isolate the grid points near the interface, a δ function as described in Refs. [45–47] can be used to locate the interface as well as to calculate the surface or line integral along the interface. The δ function is defined as:

$$\delta(\eta) = \frac{1}{2e}\left(1 + \cos\left(\frac{\pi\eta}{e}\right)\right) \quad -e < \eta < e \tag{14a}$$

$$\delta(\eta) = 0 \qquad else \tag{14b}$$

where $e = 0.2$ is chosen such that the delta function samples two or three points across the interface [47]. The line integral of a 2-D grain boundary, i.e. its length, is simply the sum of the δ values. The boundary curvature at individual grid points along the boundary is weighted by its corresponding δ value. This is done on a grain-by-grain basis and yields all of the curvature values. This list can be used to create a curvature distribution for the entire polycrystalline system. The distribution must thus be nearly symmetric since the curvature is calculated twice for each boundary, once with positive curvature and once with negative curvature. To avoid TJs, voxels with a sum of the order parameters of $\Phi > 1.01$ were filtered out. The curvature values are normalized by the average curvature for that timestep, such that comparisons can be made between timesteps.

In these simulations, the order parameters are fixed along the sides of the computational box. For analysis, a bounding box is defined that encapsulates grains more than two average grain sizes away from the boundary. Furthermore, the size of each grain is weighted by a factor relating to its size, due to the fact that larger grains are preferentially removed from the bounding box [48]:

$$F = \frac{W_x W_y}{(W_x - F_x)(W_y - F_y)} \tag{14c}$$

where W_x and W_y are the dimensions of the bounding box, and F_x and F_y are the maximum projected dimensions of each grain.

3. Simulations

3.1. Tricrystal simulation

A standard finite-difference forward-Euler representation of the evolution equations for the order parameters is used. The grid space, $dx = 0.4$, is chosen to resolve the peak in the order parameters near trijunctions. Away from the boundaries and trijuctions a sparse matrix approach is used [49]. The code is parallelized over MPI [50].

The model is validated by simulating the evolution of tricrystals with the geometry in Fig. 1(a). Values of 1.0, 0.1, 0.01 and 0.002 were chosen for L_{TJ}. The initial length of the grain in the direction of motion was set to be 10 times the grain size so that there was enough time and space for the tricrystal to converge to a steady-state shape. Once this steady state was reached, the angle, θ_a, was calculated by fitting the grain boundary shape with the theoretical shape given by Eq. (1) [2,15]. In particular, a code looped through multiple values of θ_a and a (the grain size) until the sum of the squares of the difference between the simulation shape and the theoretical shape was minimized. We found that this approach yielded the most accurate values of the trijunction angle and grain size.

Fig. 3 illustrates the close match between the theoretical shape and the simulated shape. Such close fit was achieved for all computer simulations. For simulations with no TJ drag, the value of θ_a converges to 60° as the grain size is increased.

It is clear from Fig. 4 that the TJ mobility converges as the grain size to interface width ratio increases. The interface width is, by convention, the number of grid points between 0.1 and 0.9, or approximately 8 grid points. The TJ mobility, m_{TJ}, converged to values of approximately 0.228, 0.060, and 0.036 for L_{TJ} values of 0.1, 0.01, and 0.002, respectively. Importantly, the convergence of the TJ mobility means that the velocity is proportional to $(2\cos\theta - 1)$, suggesting that the deviation of the TJ dihedral angles from equilibrium is now a driving force for boundary motion. Grain boundary curvature still contributes, but the TJ mobility slows the velocity and decreases the angle. This calculation also allows us to choose interfacial widths sufficiently small to ensure that interfacial thickness has a negligible effect on the results of the calculations.

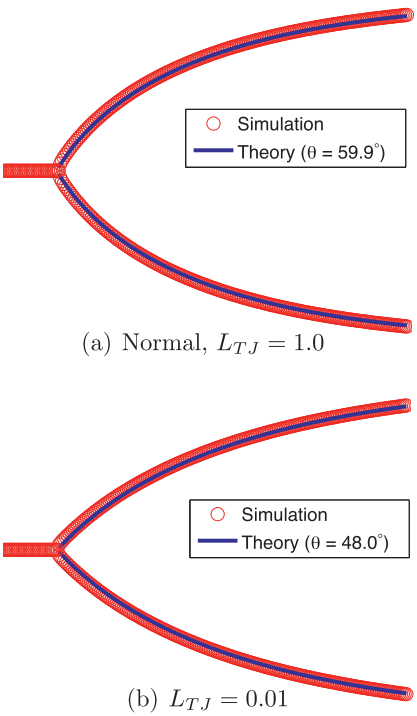

Fig. 3. Grain boundary shape of tricrystals, from both simulation and theory. The fitted angles are approximately 59.9° (a) and 48° (b) for grain boundary-limited and TJ-limited ($L_{TJ} = .01$), respectively.

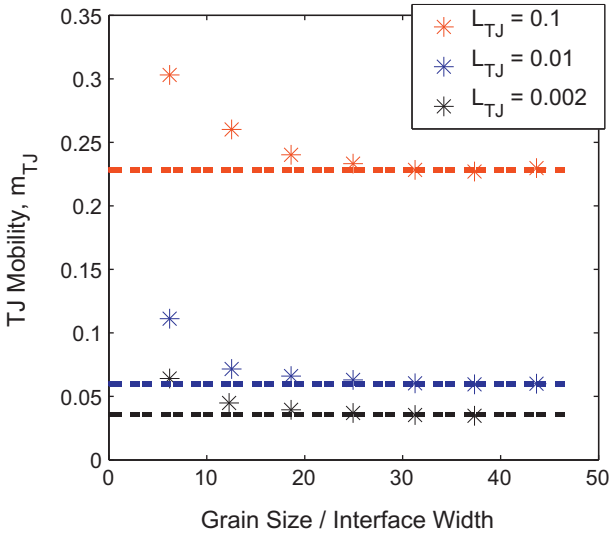

Fig. 4. Plot of dimensionless TJ mobility vs. dimensionless grain size. The TJ mobility converges at a grain size of approximately 20 times the interface width.

3.2. N-sided grain simulation

The evolution of four-sided and five-sided grains was also determined, both to verify the TJ mobilities, m_{TJ},

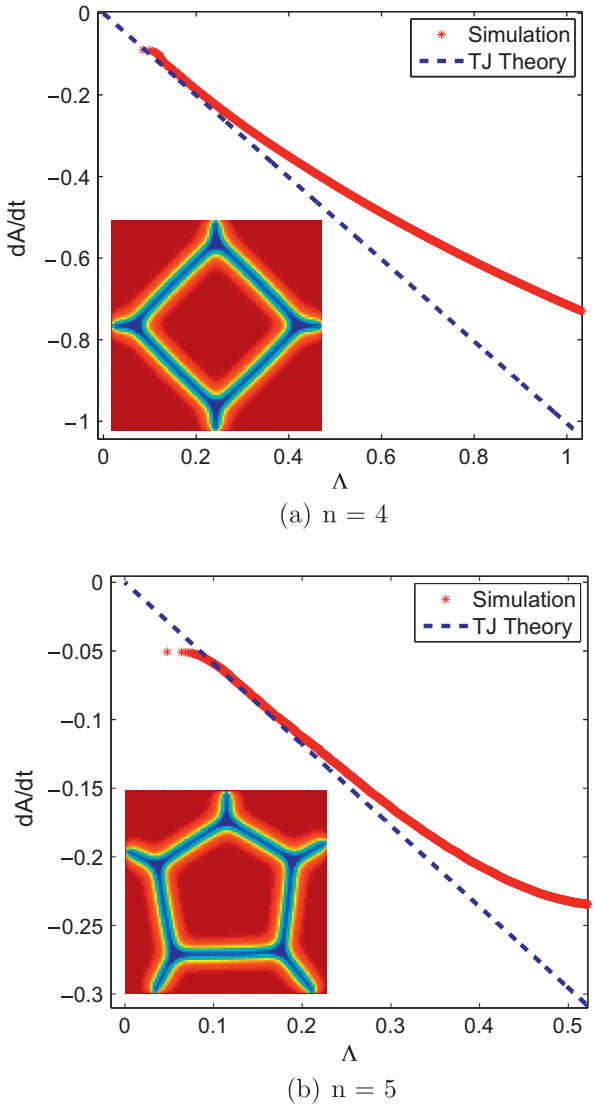

Fig. 5. Four-sided and five-sided grain simulations for $L_{TJ} = 0.001$. In both cases, the simulation matches or approaches the TJ-limited theory.

calculated in the previous section as well as to validate the TJ kinetics theory, Eq. (8), proposed by Gottstein and Shvindlerman [15]. See Fig. 5 for the geometry used in these simulations.

For grain boundary-limited simulations, i.e. $L_{TJ} = 1.0$, the growth rate of the grain area, dA/dt, is found to be within 5% of the Von Neuman–Mullins values.

For $L_{TJ} = 0.001$, the simulations matched or approached the TJ-limited theory [18] for four- and five-sided grains (see Fig. 5). The values of m_{TJ} were taken from the converged tricrystal results to calculate Λ. For the four-sided grain, for example, agreement between the simulation and theory was obtained for Λ less than approximately 0.3. However, for very small grain sizes, where Λ is less than 0.1, the shrinkage rate began to deviate from the theory. This maximum corresponds to a TJ spacing of approximately 4.0 times larger than the interface. The TJ spacing, a, was approximated as the distance between TJs for regular polyhedra for a calculated area. This deviation from theory for very small grains where Λ is less than 0.1 is likely due to a combination of TJ mobility fields beginning to overlap as well as large interface widths relative to grain size. Furthermore, this minimum is smaller than for grain boundary-limited growth, in which the four-, five- and eight-sided grains must have TJ spacings of approximately 6.1, 5.1 and 4.5 times larger than the interface, respectively. This difference in Λ validity threshold for grain boundary- and TJ-limited growth is likely due to the velocity. Grain boundary-limited grains will accelerate as they shrink due to the increasing curvature and driving force, introducing greater numerical errors that accumulate as the velocity increases. TJ-limited grains, however, theoretically shrink at a constant, and slower, velocity. Thus, the agreement between the theory and simulation for small shrinking grains is better in the TJ-limited regime than in the grain boundary-limited regime.

Two- and three-sided grains, due to their smaller TJ spacing and higher velocity, will thus contribute the largest error, or deviation from the TJ kinetics theory, as Λ becomes small and they shrink and disappear. As long as the average grain size is 5–10 times greater than the interface width, then this error is assumed to be insignificant, especially considering the small fraction of three-sided grains (<5%) in a 2-D polycrystal [32].

Overall, this TJ mobility-limited phase-field model has been shown to be consistent with previous results in the

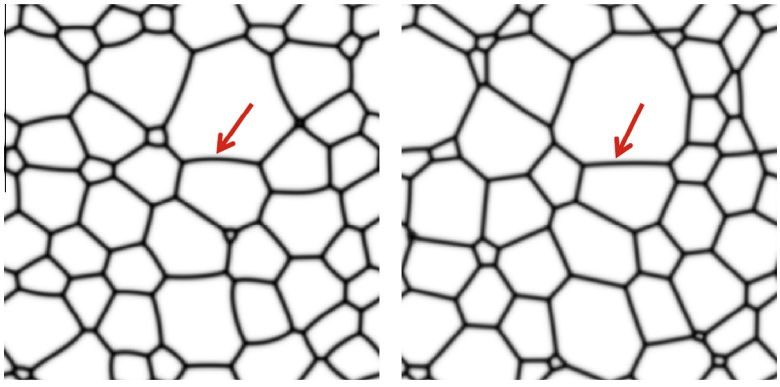

Fig. 6. Comparison of grain growth simulation for grain boundary-limited, $L_{TJ} = 1.0$ (left), and TJ-limited, $L_{TJ} = 0.01$ (right). Arrow indicates a curved vs. nearly straight grain boundary in the grain boundary-limited and TJ-limited simulation images, respectively.

literature, at least for two-, four- and five-sided grains. In particular, it is clear that the TJ dihedral angles deviate from equilibrium and move at a rate proportional to $(2\cos\theta - 1)$. Moreover, grain boundary mobility is completely unaffected by the presence of trijunction drag. Thus, it is possible to examine intermediate values of L_{TJ}, where there are two competing driving forces for grain growth whose relative importance is a function of the grain size.

3.3. Polycrystalline simulations

Polycrystals of 10^4 grains were simulated with a grid size of 2048×2048 and fixed boundary conditions. Simulations were done with $L_{GB} = 1.0$ and L_{TJ} values of $10^0, 10^{-1}$ and 10^{-2}, corresponding to initial Λ' values of ∞, 1.59 and 0.35, respectively. In order to simulate even smaller TJ mobility within a reasonable computation time, a smaller simulation of 512×512, with 10^3 grains, was done for $L_{TJ} = 10^{-3}$ and $\Lambda' = 0.08$.

Lower values of L_{TJ} resulted in slower growth rates, as expected. The average grain size over time is plotted in Fig. 7. The grain growth exponents were found using a best-fit calculator $(R(t) = At^n + R_0)$ in MATLAB. These fits provided values for R_0, the initial average radius and y-intercept, which were used to calculate and plot $ln(R - R_0)$ vs. $ln(t)$, seen in Fig. 7(b). For each dataset, the slope of the log–log data matches the exponent from the fit.

The grain boundary-limited simulations ($L_{TJ} = 1.0$) had a growth exponent of 0.49, which is consistent with the theoretical value of 0.5 for curvature-driven grain growth. The $L_{TJ} = 10^{-3}$ simulation had a growth exponent of 1.05, which is consistent with the theoretical value of 1.0 for TJ mobility-limited growth. Furthermore, as the average grain size increases, the effect of TJ mobility decreases because the parameter of importance, Λ', couples the TJ mobility with the grain size. Theoretically, the exponent of both simulations should converge to 0.5 at infinite time.

As L_{TJ} was decreased, the grain boundary curvatures approached zero, as can be seen qualitatively in Fig. 6. This suggests that for low TJ mobility, grain boundary curvature plays a small role; TJ dihedral angles become the driving force for grain growth. To quantify the effect on boundary curvature, the boundary curvatures were calculated for each run at several timesteps.

The grain boundary-limited simulation was observed to have a steady-state curvature distribution (see Fig. 8(a)). As the TJ mobility is decreased, the curvature distribution shifts towards zero curvature, but approaches the GB-limited steady-state curve as simulation time increases. For the smallest TJ mobility employed, the distribution of curvature is initially quite narrow. However, some grain boundaries clearly have non-zero curvature. This is because, although a small average value of Λ' was employed, there are grains in the system for which Λ is not small, and thus some boundaries are partially limited by boundary curvature. As time progresses, more grains

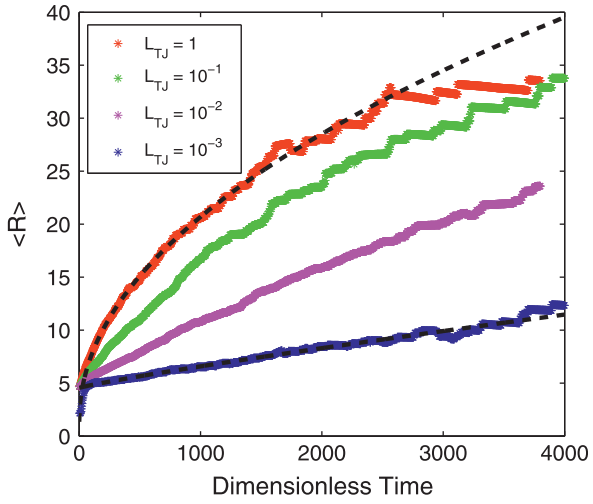

(a) Average grain radius vs. time

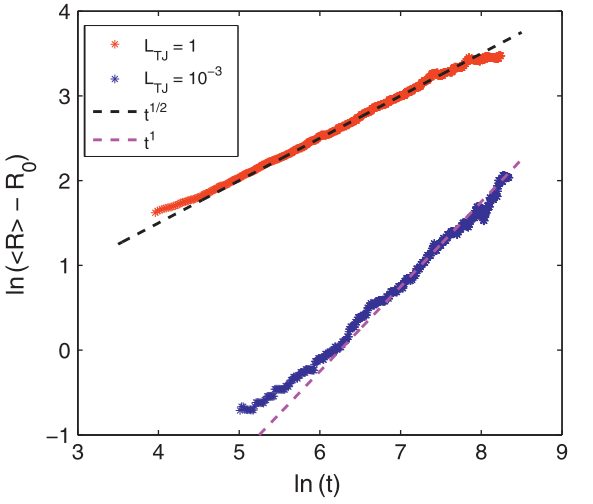

(b) $ln(R - R_0)$ vs. $ln(time)$

Fig. 7. Plot of average grain radius vs. time (a) and plot of the log of grain radius vs. log of time, illustrating $t^{1/2}$ kinetics for grain boundary-limited grain growth and t^1 kinetics for TJ-limited grain growth. For mixed kinetics, the temporal exponent lies between 0.5 and 1.

move within this limit and thus the curvature distribution is never time independent. As expected, since Λ' increases with time, all of the simulations will reach a steady-state distribution of curvature that matches the grain boundary-limited curve.

The area rate of change, dA/dt, was calculated for individual grains at each timestep. Λ was calculated using Eq. (3), where a is the approximate TJ spacing for a regular polyhedra in that grain class. Topological transitions were explicitly avoided in this calculation by requiring that the number of sides of a grain does not change when dA/dt was determined.

As a check of the method, we examine the case of grain boundary-limited simulation and compare this to the predictions of Von Neumann–Mullins (VNM). As shown in Fig. 9(a) the values for the average rate of area change,

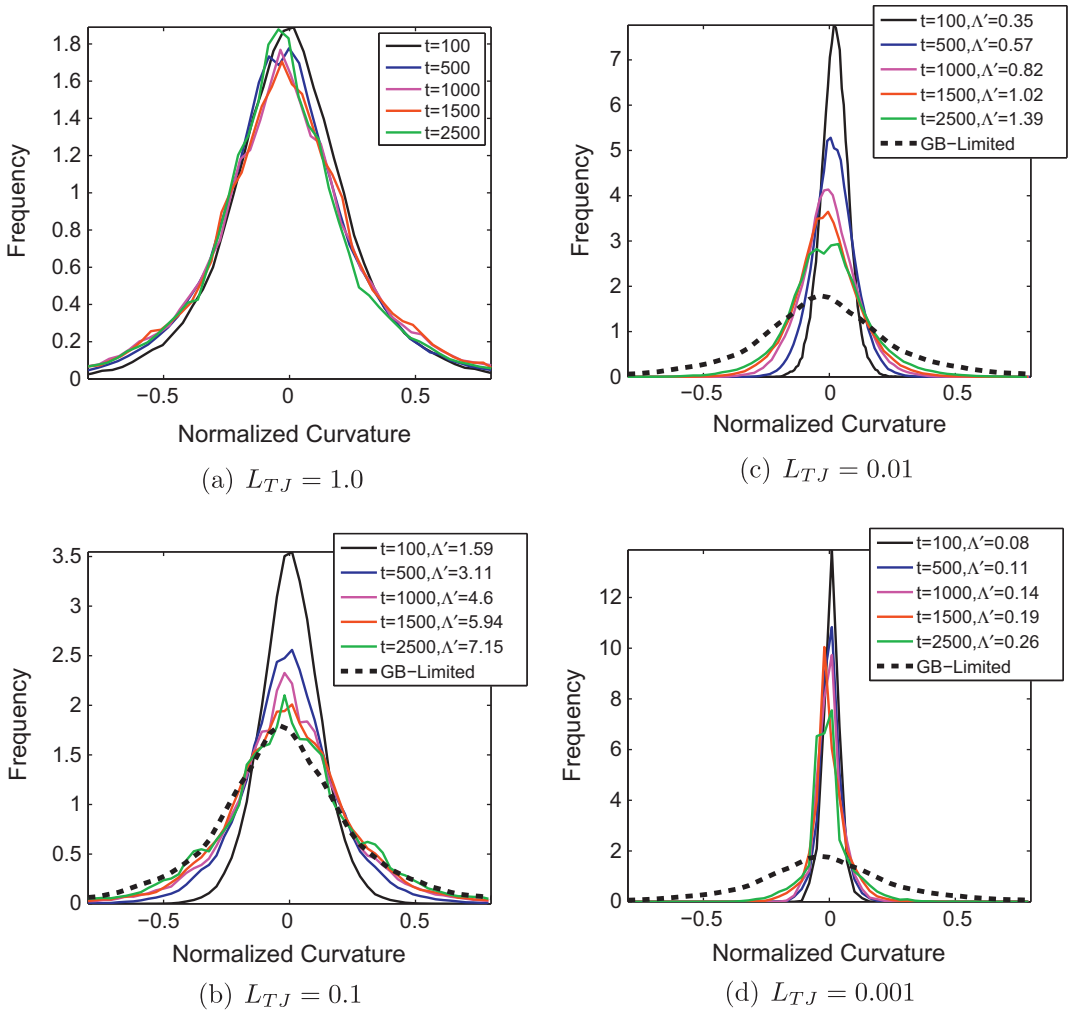

Fig. 8. Grain boundary curvature histogram for each run. The grain boundary-limited simulations (a) exhibit a steady-state curve. In the TJ-limited simulations (b–d), the histogram approaches the grain boundary-limited steady-state curve as time goes on.

$\langle dA/dt \rangle$, obtained in the simulation are very close to the predicted values.

The $\langle dA/dt \rangle$ values in the TJ-limited simulations are plotted in Fig. 9. Each point represents an average of multiple grains with similar values of Λ; the Λ bin size was chosen to be roughly constant on a log scale. The $L_{TJ} = 10^{-3}$ results were seen to match the TJ kinetics theory, Eq. (8), especially for grains with fewer than six sides. As Λ increases, which is due to the grain size increasing or the TJ mobility increasing, the growth rates underwent a transition from the TJ kinetics theory to the mixed kinetics theory, Eq. (7b). The $L_{TJ} = 10^{-1}$ results mostly match the mixed kinetics theory, especially for large grains with more than six sides. The grain classes with fewer than six sides were thus skewed towards the TJ kinetics-limited growth theory, while the grains with more than six sides were skewed towards the mixed kinetics theory. This is consistent with the theory that grains with smaller Λ are more affected by TJ mobility.

Grain size distributions were calculated at various times. The grain boundary-limited simulations achieved a steady-state distribution, as expected. As can be seen in Fig. 10(a), lower TJ mobility results in a slightly wider grain size distribution relative to the steady-state grain boundary-limited distribution. Near the beginning of the simulations, the distribution is narrow, reaches the grain boundary-limited distribution, and then slightly broadens further. For the parameter regime examined, the distributions in the TJ-limited cases do not reach steady state. However, the grain growth exponent remains close to 1 during this evolution of the grain size distribution.

The distribution of the number of sides per grain for TJ-limited grain growth is quite similar to that for grain boundary-limited growth (see Fig. 10(b)). Unlike the grain size distribution, the topology does approach steady state.

4. Discussion

A phase-field method has been developed that captures the effects of trijunction drag on grain growth. While the calculations reported here are two-dimensional, the formulation is also valid in three dimensions. The flexibility of the phase-field method allows this approach to be used as a starting point for adding other effects, such as bulk

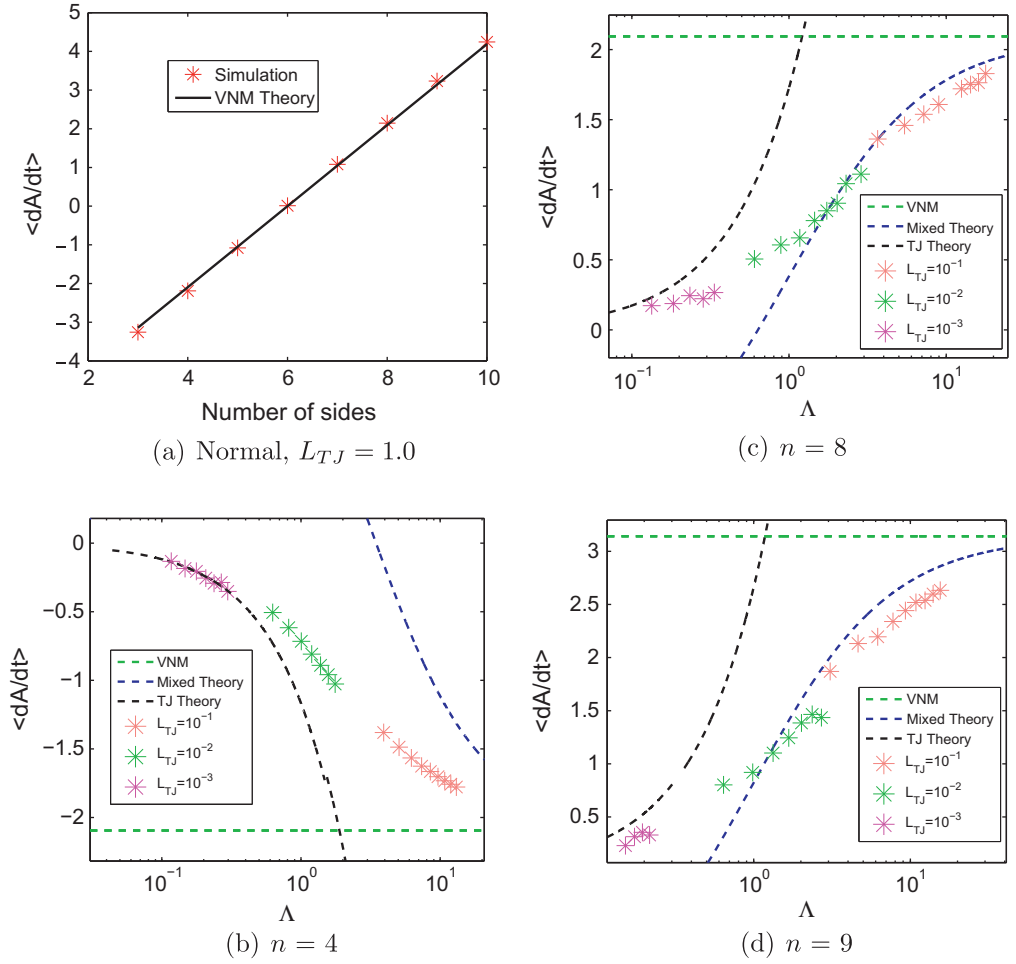

Fig. 9. (a) Plot of $\langle dA/dt \rangle$ as a function of the number of sides for grain boundary-limited growth; values match the VNM. The growth rate vs. Λ for four (b), eight (c) and nine (d) sides. The values show a smooth transition from the TJ kinetics theory to the mixed kinetics theory to the VNM.

diffusion [51–53] and grain boundary energy anisotropy. Thus, it is possible to examine the role that bulk diffusion plays in trijunction drag as well as the role of crystallography in TJ-limited grain growth.

The growth rate of grains has been shown to transition between two TJ kinetics theories and approach the VNM values. This transition between multiple theories for TJ-limited growth has not been seen before. Currently, it is clear that no single theory accurately predicts the growth rate and that the relative effects of grain boundaries and TJs are still partially unknown. This uncertainty, i.e. lack of a single unifying theory for TJ kinetics, may be partially explained by the size dependence of TJ mobility. In other words, TJ-limited growth is inherently more complex than grain boundary-limited growth because it lacks self-similarity and thus has different kinetics for smaller grains compared to larger grains.

The slight deviations from the $n = 8$ and $n = 9$ mixed kinetics theory for the $L_{TJ} = 10^{-1}$ simulations are likely due to grain size effects, i.e. when one side of a grain is roughly the size of the interface width. Deviations from theory may also have been introduced due to assumptions in the dA/dt calculations, such as the approximation as regular polyhedra in the TJ spacing calculation.

The self-similarity in grain boundary-limited growth is most clearly seen in the curvature distribution. For decreasing TJ mobilities, the deviation from the self-similar curve increases. For extremely low TJ mobility, the curvature distribution approaches a delta function at $H = 0$, and yet the kinetics are still not self-similar because the distribution still changes as the average grain size increases. This suggests that models must always incorporate grain boundary curvature, even when dealing with low TJ mobility.

The grain size distribution roughly matches that seen in Weygand et al.'s TJ-limited Potts model [30,33] for intermediate values of Λ'. It is expected that if L_{TJ} were to decrease further, the distributions would widen further. Note, however, that the TJ-limited distributions are probably time dependent. Similar to the curvature distributions, the distributions would likely approach the GB-limited distribution at longer simulation times and thus there is no steady-state regime. It is conceivable that if the TJ mobility was low enough, a steady-state distribution would be achieved. Interestingly, though, the distribution of the

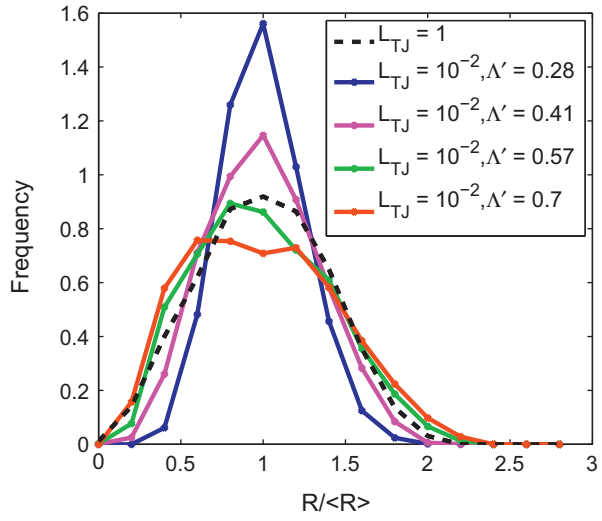

(a) Size distribution

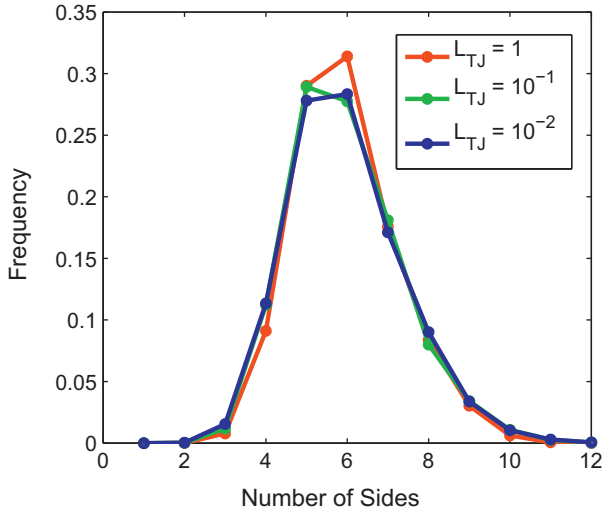

(b) Number of Sides Distribution

Fig. 10. (a) Steady-state grain boundary-limited distribution with TJ-limited distribution at various times. Lower TJ mobility results in a wider distribution. (b) Distribution of the number of sides, at steady state, illustrating that the topology is mostly independent of TJ mobility.

number of grain sides is similar for all of the simulations. The topology thus appears to be independent of the TJ mobility, at least for the values used in these simulations.

TJs may help explain some of the unusual results seen in nanocrystalline materials, including grain stabilization and linear kinetics. However, linear kinetics are not always observed in nanocrystalline grain growth, and thus there may be many other competing factors that drive grain growth at such small scales. For instance, impurity segregation may play a large role in determining relative mobilities of junctions. As such, it is possible that the impurity levels in materials could be explicitly set in order to set the driving force for grain growth [3]. Second-phase particles may also result in pinning effects that are qualitatively similar to TJ drag but differ in the way they affect grain boundary curvatures and mobilities.

Extrapolating this work into three dimensions, triple lines *and* quadruple junctions (QJs) play an important role in nanocrystalline grain growth [54,3]. In the same way that low TJ mobility results in low grain boundary curvature, low QJ mobility results in low triple-line curvature. The relative effect of each type of junction is a function of the temperature, the grain size, the impurity concentration and possible other forces. Because the activation energy for QJ mobility is relatively high, QJs may in practice be considered infinitely mobile in many systems, just as TJs are often assumed to have infinite mobility. However, any system of grains undergoing growth must contain a certain fraction of very small grains. The smaller the grain, the more it is affected by TJ and QJ mobility. Any evolving system of grains or interfaces will thus be affected by TJ or QJ mobility in some way.

5. Conclusions

We have developed a phase-field model that includes TJ mobility. The approach is consistent with theories for the motion of grain boundaries in systems with simple grain configurations. Our findings are as follows:

- The method captures the well-known linear grain growth rate of the average grain size for small TJ mobility.
- The model can capture the transition from TJ-limited mobility to classical grain boundary energy-driven grain growth as the grain size increases.
- Steady-state grain boundary curvature distributions were not observed for intermediate or even low TJ mobility. By contrast, a steady-state distribution was observed for grain boundary energy-driven grain growth.
- Despite the lack of self-similarity in the morphology of the grain boundaries with TJ-limited growth, the growth exponent for the average grain size was close to the theoretically predicted value of 1.
- Lower TJ mobility tends to result in broader grain size distributions and the topology of the grain structure is independent of the TJ mobility, within the parameter range employed in the simulations.

Acknowledgement

Funding for this research is provided by a National Science Foundation graduate research fellowship.

References

[1] Fortier P, Palumbo G, Bruce GD, Miller WA, Aust KT. Scr Mater 1991;25(1):177–82.

[2] Czubayko U, Sursaeva VG, Gottstein G, Shvindlerman LS. Acta Mater 1998;46(16):5863–71.
[3] Gottstein G, Shvindlerman LS. Boca Raton, Grain Boundary Migration in Metals: Thermodynamics, Kinetics, Applications, FL: CRC Press; 2009.
[4] Palumbo G, Thorpe SJ, Aust KT. Scr Mater 1990;24(7):1347–50.
[5] Horváth J, Birringer R, Gleiter H. Solid State Commun 1987;62(5):319–22.
[6] Bokstein B, Ivanov V, Oreshina O, Peteline A, Peteline S. Mater Sci Eng A Struct Mater 2001;302(1):151–3.
[7] Chellali MR, Balogh Z, Bouchikhaoui H, Schlesiger R, Stender P, Zheng L, et al. Nano Lett 2012;12(7):3448–54.
[8] Palumbo G, Aust KT. Mater Sci Eng A Struct Mater 1989;113:139–47.
[9] Shvindlerman LS, Gottstein G. Z Metall 2004;95(4):239–41.
[10] Von Neumann J. Metal Interfaces 1952:108.
[11] Chokshi AH. Scr Mater 2008;59(7):726–9.
[12] Stender P, Balogh Z, Schmitz G. Ultramicroscopy 2010:1–6.
[13] Gottstein G, Shvindlerman LS, Zhao B. Scr Mater 2010;62(12):914–7.
[14] Portavoce A, Chow L, Bernardini J. Appl Phys Lett 2010;96(21):214102–214102–3.
[15] Gottstein G, Ma Y, Shvindlerman LS. Acta Mater 2005;53(5):1535–44.
[16] Protasova SG, Gottstein G, Molodov DA, Sursaeva VG, Shvindlerman LS. Acta Mater 2001;49(13):2519–25.
[17] Shvindlerman LS, Gottstein G. Mater Sci Eng A Struct Mater 2001;302(1):141–50.
[18] Gottstein G, Shvindlerman LS. Acta Mater 2002;50(4):703–13.
[19] Upmanyu M, Srolovitz DJ, Shvindlerman LS, Gottstein G. Acta Mater 2002;50(6):1405–20.
[20] Mattissen D, Waero A, Molodov DA, Shvindlerman LS, Gottstein G. J Microsc 2004;213(3):257–61.
[21] Zöllner D. Comput Mater Sci 2011;50(9):2712–9.
[22] Barrales-Mora LA, Gottstein G, Shvindlerman LS. Acta Mater 2012;60(2):546–55.
[23] Weygand D, Bréchet Y, Lepinoux J. Interface Sci 1999;7(3-4):285–95.
[24] Krill III CE, Helfen L, Michels D, Natter H, Fitch A, Masson O, et al. Phys Rev Lett 2001;86(5):842–5.
[25] Paul H, Iii CEK. Scr Mater 2011;65(1):5–8.
[26] Farkas D, Mohanty S, Monk J. Phys Rev Lett 2007;98(16).
[27] Saldana C, Murthy TG, Shankar MR, Stach EA, Chandrasekar S. Appl Phys Lett 2009;94(2):021910.
[28] Upmanyu M, Srolovitz DJ, Shvindlerman LS, Gottstein G. Interface Sci 1999;7(3-4):307–19.
[29] Gottstein G, Shvindlerman LS. Mater Sci Technol 2005;21(11):1261–6.
[30] Zöllner D. Scr Mater 2012.
[31] Chen LQ, Yang W. Phys Rev B 1994;50(21):15752.
[32] Fan D, Geng C, Chen LQ. Acta Mater 1997;45(3):1115–26.
[33] Weygand D, Bréchet Y, Lepinoux J. Acta Mater 1998;46(18):6559–64.
[34] Novikov VY. Scr Mater 2005;52(9):857–61.
[35] Gottstein G, Shvindlerman LS. Scr Mater 2006;54(6):1065–70.
[36] Phani M, Lebowitz JL, Kalos M, Penrose O. Phys Rev Lett 1980;45(5):366–9.
[37] Kawasaki K, Nagai T, Nakashima K. Philos Mag (Abingdon) 1989;60(3):399–421.
[38] Enomoto Y, Kato R. Acta Mater 1990;38(5):765–9.
[39] Fortes M, Ferro A. Acta Mater 1985;33(9):1697–708.
[40] Cherkaoui M, Capolungo L. Atom Continuum Model Nanocrystall Mater 2009:81–116.
[41] Barrales-Mora LA, Gottstein G, Shvindlerman LS. Philos Mag (Abingdon) 2012;92(9):1046–57.
[42] Provatas N, Dantzig JA, Athreya B, Chan P, Stefanovic P, Goldenfeld N, et al. Jom 2007;59(7):83–90.
[43] Cahn JW, Hilliard JE. J Chem Phys 1958;28:258.
[44] Allen SM, Cahn JW. Acta Mater 1979;27(6):1085–95.
[45] Mumford D, Shah J. Commun Pure Appl Math 1989;42(5):577–685.
[46] Sussman M, Smereka P, Osher S, A level set approach for computing solutions to incompressible two-phase flow, University of California; 1994.
[47] Osher S, Fedkiw R, Level Set Methods and Dynamic Implicit Surfaces, vol. 153. Springer; 2003.
[48] Russ JC. Boca Raton, The Image Processing Handbook, FL: CRC Press; 2006.
[49] Gruber J, Ma N, Wang Y, Rollett AD, Rohrer GS. Modell Simul Mater Sci Eng 2006;14(7):1189–95.
[50] McKenna IM, Poulsen SO, Lauridsen EM, Ludwig W, Voorhees PW, 2013 [in preparation].
[51] Chen LQ, Fan D. J Am Ceram Soc 1996;79(5):1163–8.
[52] Chen LQ, Fan D. Acta Mater 1997;45(8):3297–310.
[53] Poulsen SO, Voorhees PW, Lauridsen EM. Acta Mater 2013;61:1220–8.
[54] Barrales-Mora LA, Mohles V, Shvindlerman LS, Gottstein G. Acta Mater 2008;56(5):1151–64.